PAPER

Concurrent Backscatter Streaming from Batteryless and Wireless Sensor Tags with Multiple Subcarrier Multiple Access

Nitish RAJORIA[†a)], **Yuki IGARASHI**[†], *Nonmembers*, **Jin MITSUGI**[††], **Yuusuke KAWAKITA**[†††], *and* **Haruhisa ICHIKAWA**[†††], *Members*

SUMMARY This paper proposes a novel multiple access method that enables concurrent sensor data streaming from multiple batteryless, wireless sensor tags. The access method is a pseudo-FDMA scheme based on the subcarrier backscatter communication principle, which is widely employed in passive RFID and radar systems. Concurrency is realized by assigning a dedicated subcarrier to each sensor tag and letting all sensor tags backscatter simultaneously. Because of the nature of the subcarrier, which is produced by constant rate switching of antenna impedance without any channel filter in the sensor tag, the tag-to-reader link always exhibits harmonics. Thus, it is important to reject harmonics when concurrent data streaming is required. This paper proposes a harmonics rejecting receiver to allow simultaneous multiple subcarrier usage. This paper particularly focuses on analog sensor data streaming which minimizes the functional requirements on the sensor tag and frequency bandwidth. The harmonics rejection receiver is realized by carefully handling group delay and phase delay of the subcarrier envelope and the carrier signal to accurately produce replica of the harmonics by introducing Hilbert and inverse Hilbert transformations. A numerical simulator with Simulink and a hardware implementation with USRP and LabVIEW have been developed. Simulations and experiments reveal that even if the CIR before harmonics rejection is 0 dB, the proposed receiver recovers the original sensor data with over 0.98 cross-correlation.

key words: *backscatter communication, multiple access, harmonic rejection*

1. Introduction

The integrity of civil structures, airplane, artificial satellite and machinery should be examined regularly after their construction to avoid failures and accidents. In reality, however, we occasionally see fatal accidents stemming from the lack of sufficiently frequent and detailed health checking. The major hindrances of the checking are the dependency on human intervention and labor intensive preparation.

Figure 1 shows vibrational testing of an artificial satellite. There are a number of vibration sensors attached to the body of the satellite and each sensor is connected to the power source and the signal processor. Wire harnesses shall be carefully routed not to damage the mechanical characteristics and also the delicate structure, which is labor intensive and demands a dedicated environment. This is the typical setting of vibrational testing to measure frequency response of a structure. Concurrent collection of data streaming from multiple sensors is essential to establish the frequency response of the structure against an exciting force.

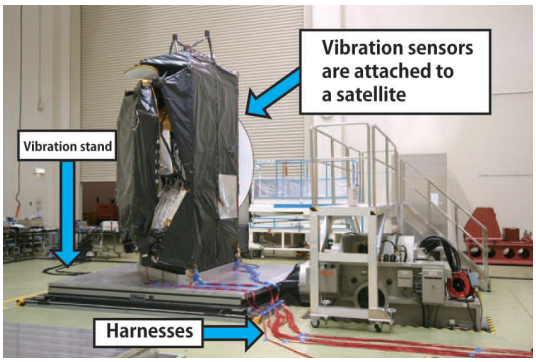

Fig. 1 An artificial satellite subjected to vibrational testing (source: Japan Aerospace Exploration Agency).

If we realize health check with wireless batteryless implanted sensors, we can examine the target structures more often and in detail with lower cost, which surely will mitigate safety risk. This is why batteryless wireless structural health check attracts significant technical interest [1]–[5]. The use of backscatter wireless communication to transfer not only unique ID of physical objects, but also sensor data is an emerging research field [6], [7].

Multiple Subcarrier Multiple Access (MSMA) have been proposed for this challenge [8], [9]. The principle is based on the backscatter wireless communication mechanism which is extensively used in passive RFID and radars [10]. The best feature of MSMA is to allow concurrent sensor data streaming from multiple batteryless sensors.

Since our previous publications have not fully addressed the interference rejection methodology and general evaluations, we describe the details of MSMA in this paper. To facilitate the discussion, we first explain the backscatter communications principle, then introduce the concept of MSMA and the related work.

1.1 Backscatter Wireless Communications Principle

A typical backscatter wireless communications system is

Manuscript received December 13, 2016.
Manuscript revised April 27, 2017.
Manuscript publicized June 13, 2017.

[†]The authors are with Graduate Student, Graduate School of Media and Governance, Keio University, Fujisawa-shi, 252-0882 Japan.
[††]The author is with Faculty of Environment and Informations Studies, Keio University, Fujisawa-shi, 252-0882 Japan.
[†††]The authors are with Department of Human Communications, University of Electro-Communications, Chofu-shi, 182-8585 Japan.
a) E-mail: nitish@keio.jp

DOI: 10.1587/transcom.2016EBP3472

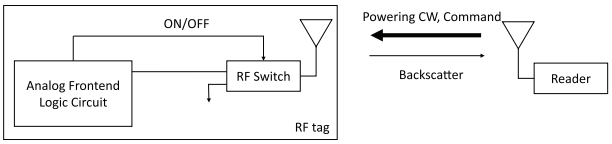

Fig. 2 Passive RFID enables a batteryless RF tag to send signal by changing the antenna impedance.

passive RFID in the UHF (860–960 MHz) band. The system is extensively used in supply chain management (SCM) applications where tiny, low cost RF tags are attached to physical objects. The location and disposition of the physical objects are shared among stakeholders via a standardized information platform [10], [11]. The non-line-of-sight long range communication, fast inventory of RF tags and writing function distinguish UHF RFID from other automatic identification technology such as bar-code and NFC.

A passive RFID system comprises of a Reader/Writer and multiple RF tags. The RF tag is powered by the continuous wave (CW) provided by the Reader/Writer and processes the commands. The tag-to-reader link is established by changing the antenna impedance of the RF tag with an embedded RF switch, as shown in Fig. 2. Multiple access from RF tags to Reader/Writer is usually based on TDMA, specifically frame slotted ALOHA.

RF tag which houses a sensor and can superimpose sensor data on backscatter signal is referred to as sensor tag. When sensor data needs to be collected from sensor tags, the Reader/Writer commands the acknowledged RF tag to send sensor data. Since the existing multiple access methods in such sensor data collection state are all based on TDMA, it is difficult to send sensor streams concurrently from multiple sensor tags.

The communication distance between an RF tag and Reader/Writer is, in many cases, dominated by the reader-to-tag link, which powers RF tags. When we have a high sensitivity RF tag, the second bottleneck of reading distance is the phase noise of the Reader/Writer. Since the phase noise diminishes as we widen the frequency separation from the powering CW, many UHF RFID system employ subcarrier backscatter by superimposing a constant rate on/off keying to the digital data. The spectrum of normal backscatter and subcarrier backscatter are illustrated in Fig. 3.

The subcarrier backscatter is advantageous to avoid phase noise with the penalty of less bandwidth. With the subcarrier backscatter, we can also protect the inherently weak backscatters from neighbor Reader/Writers. Since subcarrier is produced by constant rate on/off keying without any channel filter, a subcarrier backscatter entails harmonics. Because of these harmonics, the simultaneous usage of multiple subcarriers has not been considered nor tried so far.

1.2 MSMA Overview

MSMA is a pseudo-frequency division multiple access (FDMA) using multiple subcarriers simultaneously, as

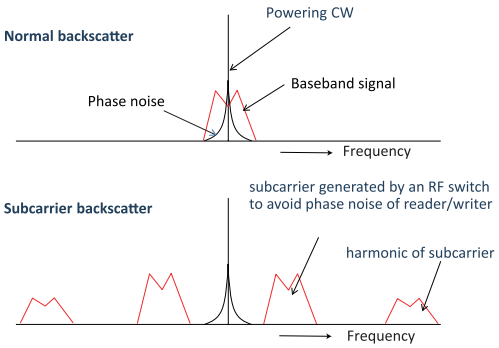

Fig. 3 By adding constant rate on/off keying to the data, we can separate backscatter signal from the phase noise of empowering continuous wave.

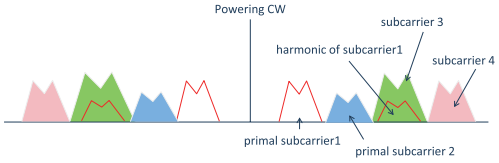

Fig. 4 MSMA uses multiple subcarriers enabling concurrent sensor data stream collection. We shall reject mutual harmonics.

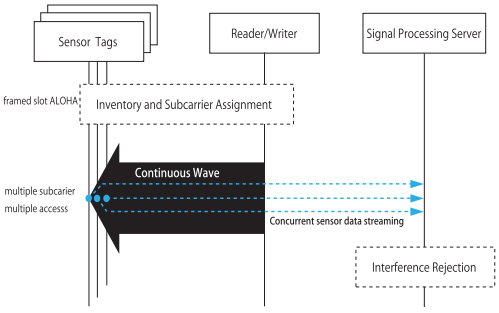

Fig. 5 Multiple subcarrier multiple access has two phases. In the first phase, the Reader/Writer inventories sensor tags with conventional frame slotted ALOHA. In the second phase, the Reader/Writer transmits continuous wave which powers sensor tags to allow concurrent data streaming from sensor tags.

shown in Fig. 4.

The high-level protocol of MSMA is shown in Fig. 5.

The Reader/Writer first inventories the RF tags with conventional frame slotted ALOHA. This way, the Reader/Writer collects all the unique IDs of RF tags in the interrogation field together with their RSSIs. After the inventory, the Reader/Writer assigns a dedicated subcarrier frequency to each sensor tag. The authors previously proposed an optimized subcarrier allocation in MSMA [12]. Next, the Reader/Writer transits into the "listen" state where the Reader/Writer receives the sensor data stream. Therefore, it is obvious that MSMA is advantageous in the applications where we demand long duration of synchronized sensor stream observation such as vibration testing of machinery and continuous surveillance and monitoring.

The superposition of the sensor stream on to the backscatter signal can be done either by digital or analog

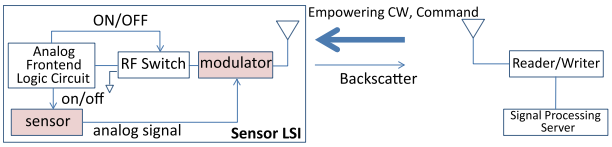

Fig. 6 A typical schematic of sensor tag in MSMA.

modulation. In digital modulation, we first sample and quantize sensor data with an analog-digital converter (AD converter). The digital sensor data is superimposed on the subcarrier by taking the exclusive OR of sensor data and subcarrier bits. In analog modulation, we can eliminate the AD converter in the sensor tag. If we develop a harmonics rejection receiver which supports concurrent analog streams, we can even apply the method to digitally modulated signal regardless of the modulation and coding scheme used. This strategy, in return, demands a sophisticated rejection method. A sensor tag in MSMA can thus be produced just by adding a sensor and a modulator to the RF tag, as shown in Fig. 6. The harmonic rejection method cancels out the mutual interference among subcarrier. Replica of subcarrier harmonics can be calculated from the primal subcarrier. The main problem in this replica generation is accurate measurements of phase delay and carrier delay of primal subcarrier as subcarrier fluctuates from the original frequency.

1.3 Related Works

Concurrent multiple access from simple sensor tags is usually realized by employing FDMA. But in the case of backscatter communication with a low function sensor tag, it is impractical, if not impossible, to implement the adaptive channel filter to realize FDMA. The concurrent data stream with TDMA demands burst transmission, which is also impracticable in low function sensor tags. There are proposals to use CDMA [13], [14] but CDMA suffers from a large number of interfering sensor tags and the transmission power control to mitigate near/far problem is difficult to implement in backscatter communications.

There have been studies to separate collided signals from multiple passive RF tags [15]–[17]. These studies assume that signals are digitally modulated and their IQ constellations are calibrated first and can be discriminated each other with the calibration. Hu [15] additionally uses the time envelop to extract collided signal information to enable concurrent sensor data streaming. Since all the existing studies are subjected to ASK, they require another IQ data calibration every time the sensor tags or the Reader/Writer change their position and orientation, not to mention the moving tags and moving Reader/Writers. The sampled and quantized sensor signal needs to be digitally superimposed onto the subcarrier signal, which inevitably expands the frequency bandwidth. Even when we assume the minimum sampling rate (double the Nyquist frequency) and 8 bits quantization. The required bandwidth expands by a factor of sixteen times compared to analog streaming.

The rejection of analog harmonics caused by the nonlinearity of amplifiers has been studied since the 1960s. Recently the use of digital signal processing for the harmonics process is studied in [18]–[20]. Although the fundamental idea of rejecting harmonics is applicable to the backscatter signals, these existing studies do not consider the phase delay, which demands delicate handling of backscatter signals as explained later in this paper.

The rest of this paper is organized as follows. In Sect. 2, we explain the principle of harmonic rejection method. In Sect. 3, the harmonics rejection performance is evaluated with simulations with Simulink and experiments using USRP and LabVIEW. Section 4 concludes the paper.

2. Harmonic Rejection Method

As we explained earlier, a subcarrier is produced by a constant rate on/off keying of antenna impedance. Figure 7 shows the general backscatter signal from a sensor tag for one period of the subcarrier. For the sake of general discussion, the phase delay of subcarrier envelope ϕ is introduced. The backscatter signal is phase modulated with sensor signal x, there is a carrier phase delay Ψ_o, and modulation index m. Since the carrier phase delay and the signal phase delay can not be separable, we denote the carrier phase shift collectively such that $\Psi = \Psi_o + x$.

Note that the subcarrier signal component is very small compared with the powering continuous wave because a subcarrier signal is fundamentally a reflection as shown in Fig. 7. Therefore, to obtain the maximum resolution of the modulated signal, the bias component of the signal is usually removed at the ingress of the receiver by applying a high pass filter (HPF). Denoting the subcarrier and the carrier angular velocities as ω_s and ω_c, respectively, the modulated subcarrier signal $S(t)$ after HPF can be written as below.

$$S(t) = \alpha \sum_{n=1,3,\cdots} \frac{1}{n} \sin(n\omega_s t - n\phi) e^{j(\omega_c t + \Psi)} \tag{1}$$

where

$$\alpha = \frac{2(1-m)}{\pi}.$$

It is shown that we inevitably produce harmonics with odd multiple of the principal subcarrier and higher harmonic produce less interference as the reciprocal of the harmonics order.

The receiver down-converts the incoming subcarrier signal $S(t)$ by multiplying the carrier signal $e^{-j\omega_c t}$ to yield the baseband IQ signal such that

$$\begin{aligned} I &= \alpha \sum_{n=1,3,\cdots} \frac{1}{n} \sin(n\omega_s t - n\phi) \cos\Psi \\ Q &= \alpha \sum_{n=1,3,\cdots} \frac{1}{n} \sin(n\omega_s t - n\phi) \sin\Psi. \end{aligned} \tag{2}$$

As a result, IQ constellation forms a straight line in the phase

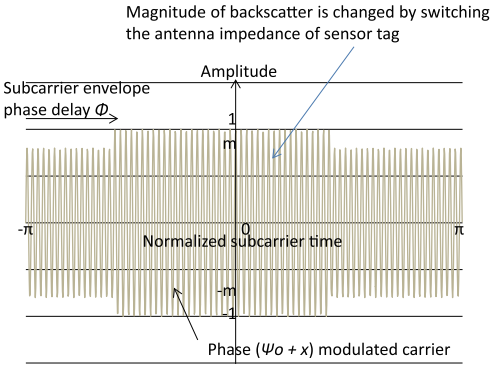

Fig. 7 A typical subcarrier wave form. The envelop is changed with a constant rate toggling of an RF switch.

plane.

The challenges in deriving harmonic replicas from a primal subcarrier signal, therefore, are summarized as follows.

- We shall handle ϕ and Ψ separately because the subcarrier phase delay ϕ in a harmonic replica shall be multiplied according to the order of harmonics to keep the linear group delay, while Ψ stays the same in all the harmonic replicas. For example, for n-th order harmonics $n\omega_s$ and the delay angle shall be $n\phi$, as shown in Eq. (1).
- We shall derive the amplitude of the primal signal to yield the predefined amplitude degradation term $\frac{1}{n}$ in Eq. (1) while the amplitude of primal subcarrier fluctuates as the IQ components move along a straight line.

The first problem can be solved by accurately measuring carrier phase shift Ψ. We apply a regression analysis with a recursive least square (RLS) filter to this problem. We develop a solution to the second problem as in the following subsection.

2.1 Replica Generation with Hilbert and Inverse Hilbert Transformations

Because the amplitude of the measured subcarrier signal fluctuates in time, the amplitude of the primal subcarrier signal should be measured and be adjusted to produce harmonics replicas. For this purpose, we introduce an analytic signal of the subcarrier with Hilbert transformation. IQ components of analytic signal of primal subcarrier (Eq. (2) where $n = 1$), denoted as $\bar{I}, \bar{Q}$, are given as follows.

$$\begin{aligned} \bar{I} &= -\alpha \cos(\omega_s t - \phi) \sin\Psi \\ \bar{Q} &= \alpha \cos(\omega_s t - \phi) \cos\Psi \end{aligned} \tag{3}$$

The combined real and analytic signal, denoted as the augmented subcarrier signal Z, rotates in the IQ plane with subcarrier frequency keeping the instantaneous amplitude constant.

$$Z = I + \bar{I} + j\left\{Q + \bar{Q}\right\} \tag{4}$$

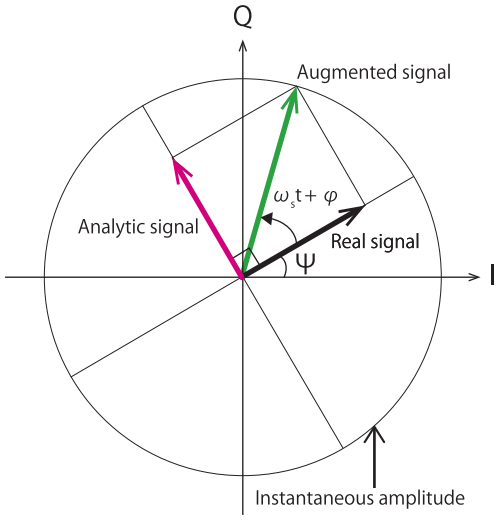

Fig. 8 Real signal and its analytic signal produced by Hilbert transformation together form the augmented signal which rotate with an instantaneous amplitude.

The harmonics of the augmented signal rotates with the angular velocity which is proportional to the order of harmonics as shown in Fig. 8. Since Ψ stays the same when we produce a harmonic, we counter-rotate the augmented signal by Ψ to obtain the following circle.

$$\begin{aligned} Z_s &= Ze^{-j\Psi} \\ &= \alpha \sin(\omega_s t - \phi) + j\alpha \cos(\omega_s t - \phi) \end{aligned} \tag{5}$$

This way, we can produce harmonics of the augmented signal, denoted as augmented harmonics, simply by multiplying the phase angle obtained, for example, by a phase locked loop (PLL) and applying appropriate scaling according to the order of harmonics.

The harmonic replica is obtained by adding the carrier phase shift Ψ and projecting the augmented harmonics to the Ψ plane. Since this projection provides the inverse operation of Hilbert transformation, we refer to this projection as Inverse Hilbert Transformation. When we denote an augmented harmonics as

$$r = r_r + jr_i, \tag{6}$$

and the unit vector of the carrier phase plane as $\cos\Psi + j\sin\Psi$, the Inverse Hilbert transformation of r, $H^{-1}(r)$, can be concisely represented by the following linear transformation.

$$\begin{aligned} H^{-1}(r) &= (r_r \cos\Psi + r_i \sin\Psi)(\cos\Psi + j\sin\Psi) \\ &= \begin{bmatrix} \cos\Psi\cos\Psi & \cos\Psi\sin\Psi \\ \cos\Psi\sin\Psi & \sin\Psi\sin\Psi \end{bmatrix} \begin{Bmatrix} r_r \\ jr_i \end{Bmatrix} \end{aligned} \tag{7}$$

2.2 Harmonics Rejection

Let us first consider a simple case, where we have a harmonic from sensor tag 1 subcarrier which interferes the primal subcarrier of sensor tag 2 as shown in Fig. 4. The augmented subcarrier signal in IQ plane is shown in Fig. 9. The

$$\begin{Bmatrix} R_1 \\ R_2 \\ R_3 \\ \vdots \\ R_9 \end{Bmatrix} = \begin{bmatrix} \sin(\omega_1 t - \phi_1) & 0 & 0 & \cdots & 0 \\ 0 & \sin(\omega_2 t - \phi_2) & 0 & \cdots & 0 \\ \frac{1}{3}\sin(3\omega_1 t - 3\phi_1) & 0 & \sin(\omega_3 t - \phi_3) & \cdots & 0 \\ \vdots & & & \ddots & \vdots \\ \frac{1}{9}\sin(9\omega_1 t - 9\phi_1) & 0 & \frac{1}{3}\sin(3\omega_3 t - 3\phi_3) & \cdots & \sin(\omega_9 t - \phi_9) \end{bmatrix} \begin{Bmatrix} A_1 e^{j\Psi_1} \\ A_2 e^{j\Psi_2} \\ A_3 e^{j\Psi_3} \\ \vdots \\ A_9 e^{j\Psi_9} \end{Bmatrix} \tag{8}$$

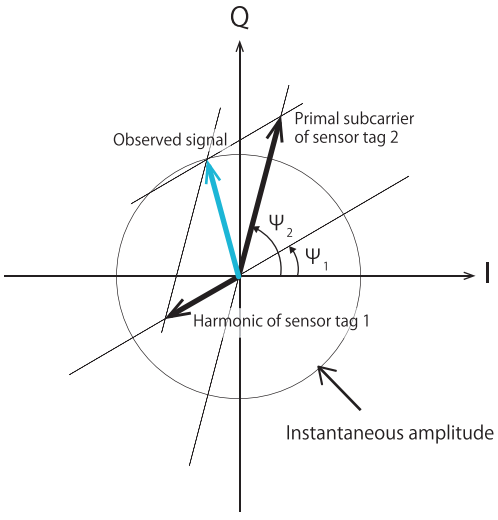

Fig. 9 The harmonic from sensor tag 1 is interfering with the primal subcarrier from sensor tag 2. The compound signal observed at the subcarrier channel of sensor tag 2.

carrier phase shifts, Ψ_1, Ψ_2 of each subcarrier are independent. The observed signal in the subcarrier channel of sensor tag 2 is the superposition of those two subcarriers. When we produce the replica of the harmonics from the primal subcarrier signal of sensor tag 1, we can recover the primal signal of sensor tag 2 by subtracting the replica from the observed signal.

Next, we consider a case where we have nine sensor tags. The nine sensor tags use different subcarrier channels from f_1 to f_9. For the simplicity, we assume sensor tag i uses subcarrier channel i without loss of generality. Each subcarrier is assumed to be modulated with an analog sensor stream. Because of the nature of the subcarrier signal, a part of harmonics of a subcarrier fall into the other sensors bandwidth such that each subcarrier produces harmonics at odd number multiples of the subcarrier frequency. Since we can remove the contribution of the envelope and carrier shift with Hilbert and inverse Hilbert transformations explained in the previous section, we only consider the modulated subcarrier signal $A_i e^{j\Psi_i}$ as the transmitted signal and R_i as the received signal where i denotes i-th subcarrier frequency. The mathematical representation of this nine sensor configuration is shown in Eq. (8).

Note that Eq. (8) is a lower triangular matrix and every instantaneous component in the matrix can be measured and sequentially computed with the procedure in the above subsections.

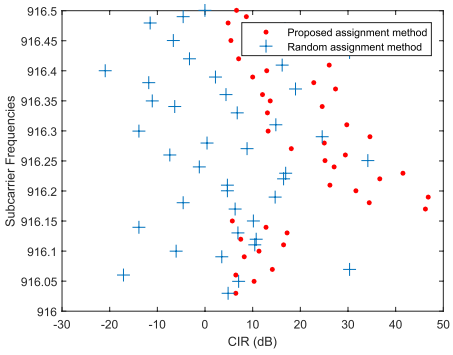

Fig. 10 CIR range can be improved by the proposed assignment method.

2.3 Carrier-to-Interference Ratio

The contribution of the harmonic rejection method depends on the original Carrier-to-Interference Ratio (CIR). The CIR of a sensor tag depends on its allocated subcarrier frequency and the distance it is located from the Reader/Writer. In [12] authors propose a subcarrier assignment method and compared with different heuristic methods to show the CIR can be improved by allocating subcarrier frequency efficiently. Figure 10 shows an example of varying range of CIR range when fifty sensor tags are allocated to subcarriers with the random assignment method and the proposed assignment method. The sensor tags are uniformly distributed in a circular area of radius 10 meter in the random fashion, the reader is located at the center. The minimum distance between a sensor tag and reader is fixed to 1 meter. It can be seen that the CIR above 0 dB when subcarrier frequencies allocated with proposed assignment method.

3. Evaluation

We implement an MSMA simulator with Simulink to verify the fundamental characteristics of MSMA and also developed an experiment system with prototype sensor tags, USRP2920 and LabVIEW. The overview of the demodulation process in both the simulator and the experimental of system for nine subcarrier channels is shown in Fig. 11.

3.1 MSMA Simulator with Simulink

The simulation on Simulink is carried out to verify the proposed fundamental MSMA demodulation process. The parameters used for the simulations are listed in Table 1. For

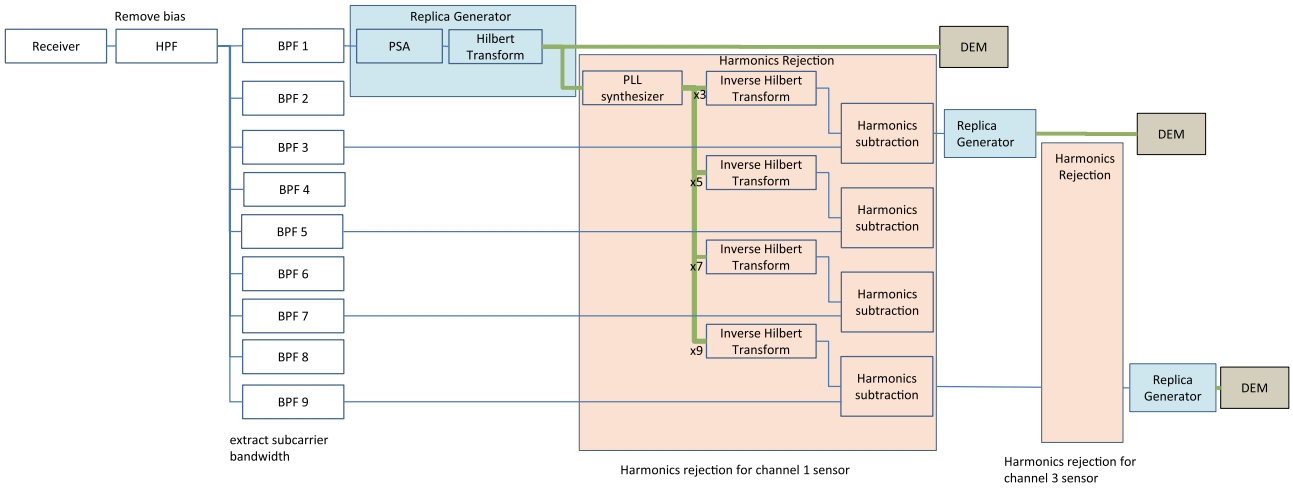

Fig. 11 Block diagram of harmonics rejection method is constructed both in Simulink and Experimental System.

Table 1 The simulation parameters.

Simulation Parameter	Value	
Subcarrier frequency	sensor tag 1	20kHz
	sensor tag 2	60kHz
	sensor tag 3	180kHz
Sensor signal (sin wave)	sensor tag 1	2kHz
	sensor tag 2	1kHz
	sensor tag 3	500Hz

the simulations we consider concurrent sensor data streaming and demodulation with 3 sensor tags whose harmonics are mutually interfering. The mutually interfering subcarrier frequencies for each sensor tag are intentionally selected to evaluate the effect of our proposed interference rejection process. The harmonic of sensor tag 1 is interfering with the primal subcarrier of sensor tag 2 and harmonics of sensor tags 1 and 2 are interfering with the primal subcarrier of sensor tag 3. In this simulation, all the replica of sensor tag 1 harmonics are calculated and subtracted first, then sensor tag 2's primal subcarrier is recovered and demodulated. Finally the replicas of sensor tag 2 harmonics is calculated and subtracted to recover and demodulate the sensor tag 3's primal subcarrier.

3.2 Experimental Evaluation with USRP and LabVIEW

For the experimental evaluation, we developed a sensor tag with a phase modulator and RF switch as shown in Fig. 12. The RF switch (PE42421SCAA-Z) is controlled by a TI MSP430. The antenna impedance of the sensor tag is changed by switching the route to open ended or terminated and the subcarrier signal is generated. The sinusoidal waveform as a sensor signal from the function generator is modulated onto the outgoing subcarrier signal by a phase shifter (Skyworks PS088-315). Each sensor signal frequency is the same as the parameters shown in Table 1.

The sensor model is not batteryless at this moment. But considering there is an experimental platform to use

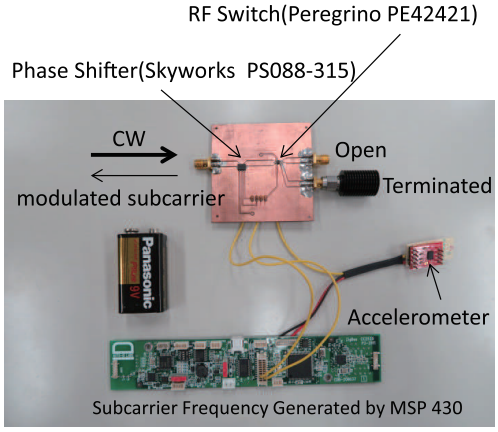

Fig. 12 A sensor model developed for the experimental verification of MSMA. Though an accelerometer is connected and it is feasible to obtain vibrational data, sinusoidal waveform generated by function generator is input as a sensor signal for this experiment in order to obtain continuous signal.

MSP430 as batteryless sensor tag [6], [21], the very low power consumption commercial MEMS accelerometer [22] and a commercial passive RF tag with accelerometer function [7], it can be said that a passively powered sensor tag could be built with current process and sensor technology.

Figure 13 shows the block diagram of the experiment setup. The signal generator generates a CW at 915MHz as a transmitted signal from Reader/Writer. The carrier signal is backscattered by the sensor tag and the subcarrier signal is combined and received by USRP2920. The USRP2920 is connected to a PC through Gigabit Ethernet cable, and IQ data are processed by a Virtual Instrument (VI) in LabView. Each sensor signal from the function generator is also measured on the VI via NI USB-6009 (DAQ in Fig. 13) and compared with the demodulated signal. The process of the VI is based on Fig. 11.

Configurations for the subcarrier frequency and the sensor signal of each sensor tag are identical to the simu-

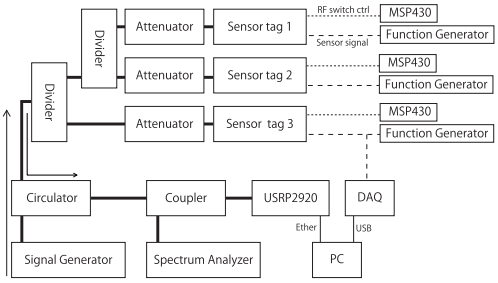

Fig. 13 Experiment setup block diagram. All components are connected with coaxial cable except a PC, MSP430s, and function generators for accurate adjustment of the signal level.

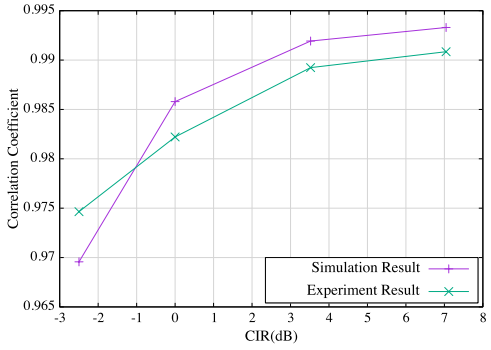

Fig. 14 A comparison of correlation coefficients derived from simulation result and experiment results corresponding to the CIR change.

lation. At the ingress of each sensor tag, a variable attenuator is installed to change the CIR that emulates the distance difference between each sensor tag and a Reader/Writer.

3.3 Result of Simulations and Experiments

In order to quantitatively evaluate the result of simulations and experiments, we derive and compare the correlation coefficients between the demodulated sensor signal and the original sensor signal at respective CIR environment as shown in Fig. 14. CIR 0 dB represents an environment in which power of the interfering signals from sensor tags 1 and 2 and the power of the desired subcarrier signal from sensor tag 3 are same. Even in case of CIR 0 dB, the correlation coefficients in both simulation and experiment are over 0.98. When it comes to CIR 7 dB the correlation coefficients are improved over 0.99 in both case.

Figure 15 shows the comparison of those signals at different CIR (0 dB, 7 dB). Even though small fluctuations are observed in the case of CIR 0 dB on the demodulated signal, still it shows good approximation to the original signal. In the case of CIR 7 dB, there is much less fluctuation compared with the case of CIR 0 dB.

4. Conclusion

Concurrent sensor data streaming from batteryless wireless sensors can be realized by using the proposed multiple subcarrier multiple access (MSMA). Because of the minimum

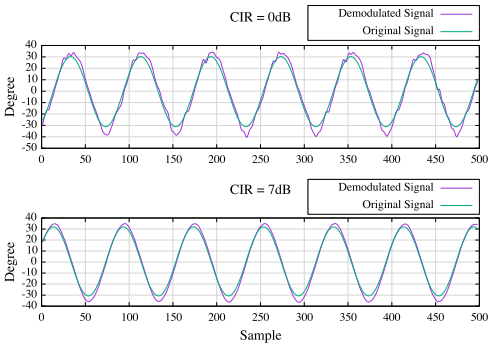

Fig. 15 Concurrently received and demodulated signal from sensor tag 3 is compared with its original signal from function generator.

functional requirements on sensors, concurrent sensor data streaming entails mutual interference. Yet, the mutual interference can be accurately rejected with the harmonics rejection receiver proposed herein. The challenges of the receiver reside in the careful handling of the phase delay of the subcarrier envelop and the carrier signal. The harmonics rejection receiver solves this problem by handling those delays in an augmented IQ signal which is produced by Hilbert transformation and projecting it back to the real IQ signal by a mathematical treatment which we refer to as inverse Hilbert transformation. By successively subtracting the harmonics replica from the received signal, we can accurately recover the original sensor data streaming at the receiver. The achieved accuracy is confirmed, both with simulations and experiment, to be above 0.98 cross-correlation even when the CIR before the harmonics rejection is 0 dB.

Acknowledgement

This work is sponsored by Ministry of Internal Affair and Communications Japan under SCOPE grant number 155003007.

References

[1] S. Adee, "Wireless sensors that live forever," IEEE Spectr., vol.47, no.2, pp.14–14, Jan. 2010.
[2] Analog Devices, MEMS wireless vibration sensing enables remote monitoring of industrial machine health, Analog device news release, June 4, 2013.
[3] Z. Wang, F. Bouwens, R. Vullers, and F. Petre, "Energy-autonomous wireless vibration sensor for condition-based maintenance of machinery," IEEE Sensors, pp.790–793, 2011.
[4] S.E. George, M. Bocko, and G.W. Nickerson, "Evaluation of a vibration powered wireless temperature sensor for health monitoring," IEEE Aerospace Conference, pp.3775–3781, 2005.
[5] M.R. Akhond, A. Talevski, T.H. Cho, "Prototype design and analysis of wireless vibration sensor," International Conference on Broadband, Wireless Computing, Communication and Applications, pp.818-0823, 2010.
[6] V. Talla and J.R. Smith, "Hybrid analog-digital backscatter: A new approach for battery-free sensing," IEEE International Conference on RFID, pp.74–81, 2013.
[7] Kineo-Battery free orientation sensor tag, http://www.farsens.com/en/product/3/kineo1-battery-free-orientation-sensor-tag. visited Dec. 10, 2016.

[8] Y. Igarashi, Y. Sato, Y. Kawakita, J. Mitsugi, and H. Ichikawa, "A feasibility study on simultaneous data collection from multiple sensor RF tags with multiple subcarriers," IEEE International Conference on RFID, pp.141–146, 2014.
[9] Y. Igarashi, N. Rajoria, J. Mitsugi, Y. Kawakita, and H. Ichikawa, "A performance analysis of interference rejection technique in multi-subcarrier multiple access," RFID Technology and Applications (RFID-TA), 2015 IEEE International Conference on. IEEE, 2015.
[10] ISO/IEC 18000-6, Information Technology - Radio frequency identification for item management -, Part 6 Parameters for air interface communications at 860 MHz to 960 MHz, (2010).
[11] GS1 EPCglobal, "The GS1 EPCglobal Architecture Framework," GS1 Version 1.7 dated 18 April 2015, http://www.gs1.org/sites/default/files/_docs/architecture/EPC_architecture_1_7-framework-May-2015.pdf
[12] N. Rajoria, Y. Igarashi, J. Mitsugi, Y. Kawakita, and H. Ichikawa, "Comparative analysis on channel allocation schemes in multiple subcarrier passive communication," IEICE Trans. Commun., vol.E98-B, no.9, pp.1777–1784, Sept. 2015.
[13] E. Vahedi, R.K. Ward, and I.F. Blacke, "Performance analysis of RFID protocols: CDMA versus the standard EPC Gen-2," IEEE Trans. Autom. Sci. Eng., vol.11, no.4, pp.1250–1261, Oct. 2014.
[14] N. Saldanha and D.C. Malocha, "Pseudo-orthogonal frequency coded wireless SAW RFID temperature sensor tags," IEEE Trans. Ultrason., Ferroelectr., Freq. Control, vol.59, no.8, pp.1750–1758, 2012.
[15] P. Hu, P. Zhang, and D. Ganesan, "Laissez-Faire: Fully asymmetric backscatter communication," ACM Sigcomm'15, pp.255–267, 2015.
[16] R. Khasgiwale, R. Adyanthaya, and D. Engels, "Extracting information from tag collisions," IEEE RFID, pp.131–138, 2009.
[17] D. Shen, G. Woo, D. Reed, A. Lippman, and J. Wang, "Separation of multiple passive RFID signals using Software Defined Radio," IEEE RFID, pp.139–146, 2009.
[18] J.A. Weldon, R.S. Narayanaswami, J.C. Rudell, L. Lin, M. Otsuka, S. Dedieu, L. Tee, K.-C. Tsai, C.-W. Lee, and P.R. Gray, "A 1.75 GHz highly-integrated narrow-band CMOS transmitter with harmonic-rejection mixers," IEEE J. Solid-State Circuits, vol.36, no.12, pp.2003–2015, 2001.
[19] C. Li, M. Li, M. Verhelst, A. Bourdoux, L. Van der Perre, and S. Pollin, "On the general mathematica framework, calibration/compensation method, and applications of non-ideal software defined harmonics rejection transceivers," IEEE Trans. Circuits Syst. I, Reg. Papers, vol.62, no.1, pp.292–301, 2015.
[20] H. Zhang, T.B. Gao, S.C.G. Tan, and O. Shana'a, "A harmonic-rejection mixer with improved design algorithm for broadband TV tuners," IEEE RFIC 2012, pp.163–166, 2012.
[21] A.P. Sample, D.J. Yeager, P.S. Powledge, A.V. Mamishev, and J.R. Smith, "Design of an RFID-based battery-free programmable sensing platform," IEEE Trans. Instrum. Meas., vol.57, no.11, pp.2608–2615, 2008.
[22] Analog Devices ADXL362 Accelerometer, http://www.analog.com/en/mems-sensors/mems-accelerometers/adxl362/products/product.html
[23] C.E. Shannon, "A mathematical theory of Communication," Bell Syst. Tech. J., vol.27, no.3, pp.379–423, 1948.

Nitish Rajoria received his Master Degree from Indian Institute of Technology, Hyderabad (IITH) India in Computer Science & Engineering. He has worked on LTE, M2M Communications. Currently, he is a Doctoral student in Keio University, Japan. His current research interest include wireless communications, RFID and information technology.

Yuki Igarashi received a Bachelor's degree and Master's degree from Keio University in 2014 and 2016, respectively. He is currently with Japan Aerospace Exploration Agency. His research interests are signal processing in wireless communications and related information technology.

Jin Mitsugi received a B.S. from Nagoya University in 1985, M.S. and Ph.D. from Tokyo University in 1987 and 1996, respectively. He was with NTT Laboratory from 1987 pursuing research and development on satellite communication system. He has been with Auto-ID Laboratory, Japan at Keio University since 2004. His research interests are network RFID, sensor network system, satellite communications and operations research

Yuusuke Kawakita received a B.A., an M.A. degree and Ph.D. from Keio University in 2000, 2002 and 2008, respectively. He is an assistant professor at the University of Electro-Communications. His present research interests focus on the ubiquitous sensing and its platform architecture.

Haruhisa Ichikawa received B.S., M.S., and Dr. Eng. degrees in electrical engineering from the University of Tokyo in 1974, 1976, and 1989, respectively. He joined NTT Laboratories in 1976, where he was engaged in fundamental research on communications software and distributed computing. He created and conducted many R&D projects for software, Internet, information sharing platform, and ubiquitous networks, including business incubation. He was Executive Director of NTT Science and Core Technology Laboratory Group till 2007, and is currently Professor at the University of Electro-Communications, Tokyo.